Atmospheric coherence time measurement by 4-aperture DIMM defocus velocity technique

M. Panahi[1], R. Shomali[2], M. Mollabashi[1,*], and Saifollah Rasouli[3,4]

[1] Department of physics, Iran University of Science and technology, Tehran, Iran
[2] Iranian National Observatory, Institute for Research in Fundamental Sciences (IPM), P.O.BOX 19395-5531 Tehran, Iran
[3] Department of Physics, Institute for Advanced Studies in Basic Sciences (IASBS), Zanjan 45137-66731, Iran
[4] Optics Research Center, Institute for Advanced Studies in Basic Sciences (IASBS), Zanjan 45137-66731, Iran
[*] Corresponding author: mollabashi@iust.ac.ir

Compiled September 29, 2019

In this work, we estimate the atmospheric Fried parameter r_0, the average wind speed $\overline{v}$ and subsequently the atmospheric coherence time τ_0 by experimental measurement via a 4- aperture differential image motion monitor (4-aperture DIMM) instrument at the Iranian National Observatory (INO) site. The experimental approach is based on the 4-aperture DIMM defocus velocity theory which uses the angle of arrival (AA) fluctuations measurement of a star light propagation through the atmospheric turbulence in form of a 4-spots configuration provided by the 4-aperture DIMM telescope. Here, we measure the defocus variance $\sigma^2_{C_4}$ and its velocity variance $\sigma^2_{\partial C_4/\partial t}$ and use the preceding theory to estimate the atmospheric turbulence parameters. We have implemented the data sampling in INO site at an altitude of 3600 m above the sea level by a 12-inch Meade Cassegrain telescope consisting a 4-aperture mask at its entrance pupil and a fast CCD camera recording short-exposure images with frame rates in a range of 480 to 620 fps from the Capella star. The experimental recorded data sets were analysed and the results were compared to that of our simulation and other methods which demonstrated a good agreement.

OCIS codes: *(010.1330) Atmospheric Turbulence; (010.7350) Wave-front Sensing;(010.0115) Imaging through turbulent media;(030.6600) Statistical optics;(080.1010) remote sensing and sensors(global).*

http://dx.doi.org/10.1364/ao.XX.XXXXXX

1. INTRODUCTION

Atmospheric turbulence has been a major problem in observatory site selection and astronomical imaging [1, 2], adaptive optics [3–5], free space communications [6–9], Optical Surveillance Systems [10] and indoor environments [11, 12]. So, a small transportable instrument is necessary to predict the quality of the image produced by telescope. In last decades, the most important atmospheric turbulence parameters such as r_0, $\overline{v}$ and τ_0 has been estimated by different methods. An enormous amount of research on conventional DIMM method [13–18] for Fried parameter r_0 and other methods [19–28] for $\overline{v}$ and τ_0 estimations has been conducted up to now, but few researchers have addressed the problem of direct estimation of averaged wind speed $\overline{v}$ over different atmospheric layers. In Lopez method [21, 29, 30], the motion velocity variance of a stellar image is measured via a small telescope with the conventional DIMM approach. Then, the covariance and structure function for the motion velocity are obtained in terms of averaged wind speed $(\overline{v})$, boiling velocity $(\overline{\triangle v})$, and averaged wind direction $(\overline{\theta})$ for a multi-layer atmospheric turbulence. At the end, the atmospheric coherence time is estimated by Roddier relation(Eq.(2)). The above method suffers from the asymmetry of the 2-aperture DIMM configuration which leads to unbiased results and also is not provided with the accurate estimation of $\overline{v}$(or v^*). On the other hand, Fast Defocus (FADE) method [24, 25] uses the atmospheric defocus of annular images and its temporal variations in a small telescope to estimate turbulence parameters which the results are good and only the experimental set up and the image processing are maybe complicated. Also, the atmospheric coherence time has been estimated with angle of arrival(AA) fluctuation measurement by Generalized Seeing Monitor (GSM) method [23]. In our previous works [31, 32], it was shown that the 4- aperture DIMM can measure the atmospheric defocus accurately and real-time. In other studies [33, 34], the inhomogeneity and anisotropy in

indoor convective and surface layer atmospheric turbulence is investigated by 4-aperture DIMM instrument. In this work, we present another simple, robust, direct and promising method based on the 4-aperture DIMM defocus velocity theory [35] recently tested at Iranaian National Observatory (INO) site to estimate r_0, $\overline{v}$ and τ_0 parameters. This method is able to overcome the asymmetry of the conventional DIMM in Lopez method and the complicated experimental setup in FADE method. First, we obtain the variance of the defocus velocity for a stellar image by a 4-aperture DIMM instrument. Then, the covariance and structure function for the defocus velocity are calculated and the atmospheric coherence time will be achieved by means of Eq.(2). In the following, we have explained the procedure. In section 2, the relations of a conventional and 4-aperture DIMM are presented to estimate the Fried parameter r_0. Then, the theory of 4-aperture defocus velocity is introduced to estimate the average wind speed $\overline{v}$ and subsequently the atmospheric coherence time τ_0. In section 3, the experiment set up and data sampling is presented. Finally, we have investigated the experimental data analysis and compared the results with other methods in section 4 and the conclusions are given in section 5.

2. THEORY

The stability of the atmosphere along the telescope line of sight to the star determines the atmospheric coherence time. The temporal fluctuations of the wavefront is caused by the wind-driven motion of a frozen layer of turbulence across the telescope. For a static one-layer model with constant speed v in front of the telescope aperture, the temporal structure function is [36]

$$D_\phi(v\tau) = \left\langle \left| \phi(x,t) - \phi(x - v\tau, t) \right|^2 \right\rangle, \quad (1)$$

where $\phi(x,t)$ is the phase at position x and time t, $\phi(x - v\tau, t)$ is the phase at different position in the pupil separated by a distance $v\tau$ and v is the wind speed. In the case of multi-layer atmospheric model, the light propagation experiences the total turbulence which the coherence time τ_0 characterizes the temporal behaviour as Roddier relation [2]

$$\tau_0 = 0.314 \frac{r_0}{v^*}, \quad (2)$$

where r_0 is the Fried parameter and v^* is the averaged wind speed $(\overline{v}_{5/3})$ [29, 30] over different atmospheric layers. So, in order to estimate the atmospheric coherence time τ_0, first we need to estimate r_0 and v^* from the experimental measurements as described below in detail.

A. Atmospheric Fried parameter r_0 estimation

We use two methods to estimate the r_0 parameter. In the first method, we use the theory of conventional DIMM [15, 16] as

$$r_{0,l} = \left[\lambda^2 \sigma_l^{-2} D^{-1/3} [0.358(1 - 0.541(B/D)^{-1/3})] \right]^{3/5}, \quad (3)$$

$$r_{0,t} = \left[\lambda^2 \sigma_t^{-2} D^{-1/3} [0.358(1 - 0.810(B/D)^{-1/3})] \right]^{3/5}, \quad (4)$$

$$r_{0,DIMM} = \frac{r_{0l} + r_{0t}}{2}, \quad (5)$$

where λ is the wavelength, D is the size of sub-apertures, B is the baseline of 4-aperture mask, σ_l and σ_t are the longitudinal and transversal variance, respectively. In the conventional DIMM method, it is essential to adjust the baseline perpendicular to wind speed direction and also to satisfy the condition $B \geq 2D$ [16] for DIMM geometrical parameters. Here, we have a 4-aperture configuration composed of two simultaneous conventional DIMM which are perpendicular to each other. So if we don't know the wind speed direction, we are likely to average the r_0 given by the horizontal and vertical sub-apertures as

$$r_{0,DIMM} = \frac{r_{0,Horizontal\ DIMM} + r_{0,Vertical\ DIMM}}{2}, \quad (6)$$

where horizontal and vertical DIMM refer to sub-apertures (α, γ) and (β, δ) in Fig.1, respectively.

In second method, we utilize a recently proposed 4-aperture defocus theory and the angle-of-arrival (AA) fluctuations data, experimentally recorded by a 4-aperture DIMM instrument. The wavefront at the telescope entrance is assumed as

$$\begin{aligned} W(x,y) &= C_2 x + C_3 y + C_4(x^2 + y^2) + C_5(x^2 - y^2) \\ &+ C_6 xy + C_7(x^2 + y^2)y + C_8(x^2 + y^2)x, \end{aligned} \quad (7)$$

where C_2 and C_3 are tip-tilt coefficients, C_4 is the defocus coefficient, C_5 and C_6 are astigmatism coefficients with the axes at 0-90 and ± 45 degrees and C_7 and C_8 are the coma coefficients along the y and x axes, respectively. In this unique method [35, 37], by using the AA fluctuations of each one of the sub-apertures, the defocus coefficient is obtained as follows

$$C_4 = -\frac{(t_{x\alpha} - t_{x\gamma}) + (t_{y\beta} - t_{y\delta})}{4 F_{tel} B}, \quad (8)$$

where α, β, γ, and δ refer to the sub-apertures, F_{tel} is the telescope focal length and B is the baseline of the 4-aperture DIMM mask. By measuring the spots displacements in x and y directions (t_x and t_y) for each one of sub-apertures and using Eq.(8), the defocus aberration coefficient C_4 is obtained. Now, we can estimate the Fried parameter r_0 in 4-aperture DIMM method as follows [37]

$$r_{0,4-DIMM} = \frac{\lambda^{6/5} (\sigma_{C_4}^2)^{-3/5}}{B^{6/5}} \left[0.0424 D^{-1/3} - 0.012 B^{-1/3} \right]^{3/5}, \quad (9)$$

where λ is the wavelength, $\sigma_{C_4}^2$ is the defocus variance , D is the telescope diameter and B is the baseline of the 4-aperture mask.

B. Averaged wind speed $\overline{v}$ estimation

The average wind speed $\overline{v}$ over different atmospheric layers is one of the most important parameters in turbulence. In 4-aperture DIMM method, for a propagation of star light through the real multi-layer atmosphere, the averaged wind speed $\overline{v}_{5/3}(v^*)$ is estimated by [35]

$$\overline{v}_{4-DIMM} = \left[\frac{\sigma^2_{\frac{\partial C_4}{\partial t}} B^2}{\lambda^2 r_0^{-5/3} (0.064 D^{-7/3} + 0.066 B^{-7/3})} \right]^{1/2}, \quad (10)$$

where r_0 refers to atmospheric Fried parameter obtained by Eqs.(3) and (4) or Eq.(9) and $\sigma^2_{\frac{\partial C_4}{\partial t}}$ refers to the defocus velocity variance which is btained by

$$\sigma^2_{\frac{\partial C_4}{\partial t}} = \frac{1}{exposure\ time} \sigma^2_{C_4}, \quad (11)$$

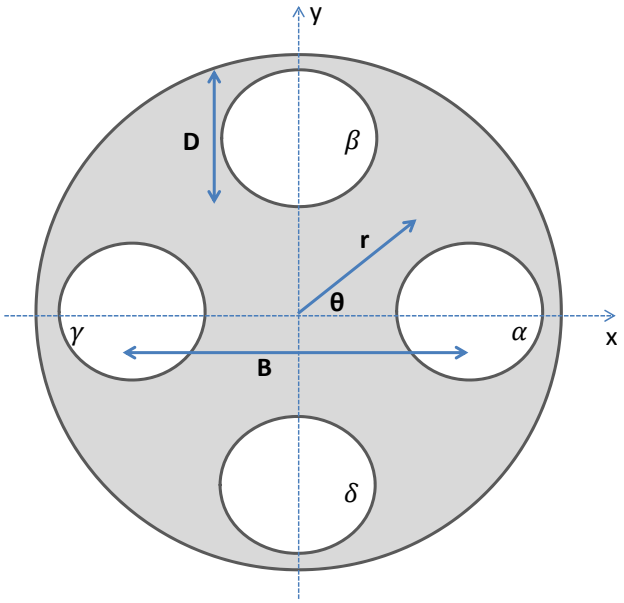

Fig. 1. Schematic illustration of a 4- aperture configuration with aperture diameters D and baseline B.

where the exposure time of imaging is needed. By substituting the $\sigma^2_{\frac{\partial C_4}{\partial t}}$, estimated r_0 and other parameters in Eq.(10), the average wind speed $\overline{v}_{4-DIMM}$ is estimated. At the end, by substituting the r_0 and $\overline{v}_{4-DIMM}$ (v^*) into Eq.(2), the atmospheric coherence time τ_0 will be estimated.

3. EXPERIMENT

For experimental measurements, we have collected the data through observations of the Capella star at the Iranian National Observatory (INO) site, which is located at latitude 33°.674 and longitude 59°.39 in the central Iran and at an altitude of 3600 m above the sea level, as shown in Fig.2. We have used a 12-inch Meade Cassegrain telescope with a 4-aperture mask to provide 4-spot images from Capella star by a fast CCD camera. Then, by measuring the defocus aberration coefficient and processing the data, the turbulence parameters r_0, $\overline{v}$ and τ_0 has been estimated according to the theory described in previous section.

A. 4-DIMM Instrument Descrption

Our measurement instrument consists a telescope, a 4-aperture mask, a detector and a laptop, as shown schematically in Fig.3. It uses a 12-inch automated Meade Cassegrain telescope with a focal length of $F_{tel} = 3.048$ m installed on an equatorial mount equipped with a 4-aperture mask at its entrance pupil. This mask enables us to obtain 4-spots images to measure the relative motion of spots and finally the defocus aberration. The subpupils are realized by four similar holes in the mask. As we adjust the focus of the telescope to a defocused mode, the 4-star image is obtained on the image detector.

The detector used is a $PL-B761$ pixelink monochrome CCD camera having a size 752×480 pixels in full frame. The large $6\,\mu$m pixel pitch and high peak responsivity enhance the camera's ability to operate in short exposures and low light levels. Each stellar image covers an area of about 11×11 pixels with a pixel angular size of 0.4 arcseconds. The quantum efficiency of the camera is 50%, readout noise is less than 1.5 DN and the exposure range is $50\,\mu$s to 2 s. By selecting a small region of interest, the exposure time of 1 to 2 ms is obtained which is most of the time short enough to freeze the turbulence effects.

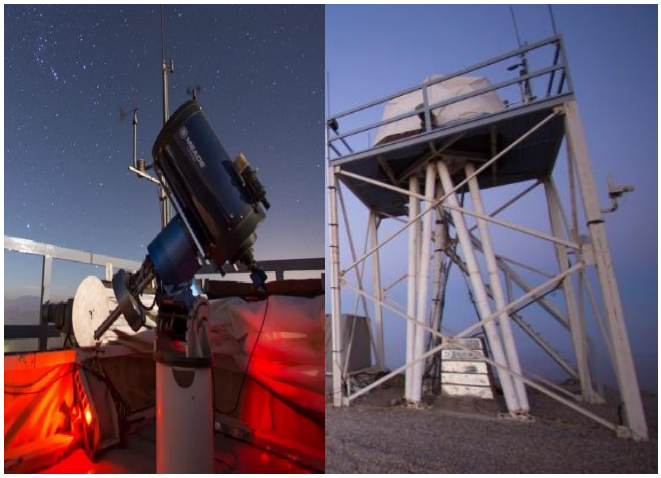

Fig. 2. 12-inch automated Meade Cassegrain telescope on the tower located at Iranian National Observatory at an altitude of 8 m above the ground and 3600 m above the sea level.

B. Data Sampling and Processing

We have obtained 157 video files from the Capella star in a 4-spot configuration which are composed of totally 157,000 frames with frame rates about 480 to 620 fps.

As illustrated in Fig.4, the position of each spot is derived by centroiding in a 12×12 pixels window. To omit the background noise from the 4-spot images, we threshold the lower intensities. Also, in some data frames, the image of a spot has been faded, in which it is necessary to omit unfavorable frames in our analysis (Fig.4(d)). Now, we are ready to measure the difference between the real and averaged position of spots (t_x and t_y for each sub-aperture) to calculate the defocus coefficient C_4 in Eq.(8). Subsequently, the defocus variance $\sigma^2_{C_4}$ and the defocus velocity variance $\sigma^2_{\partial C_4/\partial t}$ are measured for 157 image sequences of totally 157,000 frames with exposure times 1 to 2 ms.

C. Imaging Exposure Time

Through recording an image, the phase variations are integrated over the exposure time and lead to a blurred picture. The exposure time bigger than 2 ms may not be short enough to freeze the image motion. In short exposures, the contribution of the sky background to the recorded images is not significant, but maybe lead to dark frame or read out noise which must be checked. for $\overline{v}$ and τ_0 estimation, it is essential to have short-exposure imaging which depends on the turbulence conditions. the image frame rates of about at least 500 fps is needed to have a good understanding of atmospheric turbulence variations and to freeze the wind-driven motion, as mentioned above.

D. Signal-to-Noise Ratio

In the experimental measurements, the diameter of the subapertures is an important parameter in determining the signal-to-noise ratio. For an optical system, the number of detected photoelectrons in the stellar image is obtained by [38]

$$n_e = N_\gamma 10^{\frac{-M^V}{2.5}} 0.25\pi D^2 t_{exp} B_{nm}[QE \times T], \qquad (12)$$

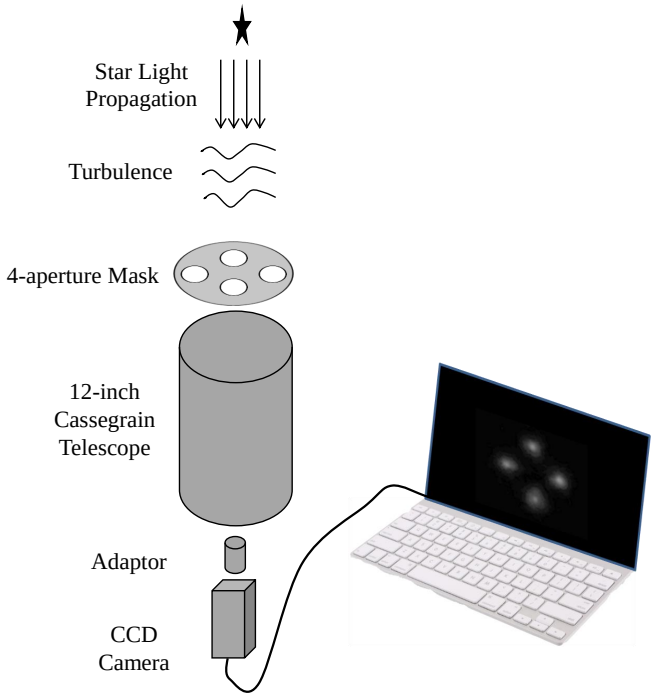

Fig. 3. The experimental set up of the instruments used in atmospheric turbulence data collection consisting of a 12-inch Meade Cassegrain telescope with focal length $F_{tel} = 3.048m$, a 4-aperture mask used at the entrance pupil of the telescope with $D = 10cm$ and $B = 20.5cm$, a high speed $PL - B761$ pixelink monochrome CCD camera and a core-i5 $K456$ ASUS laptop.

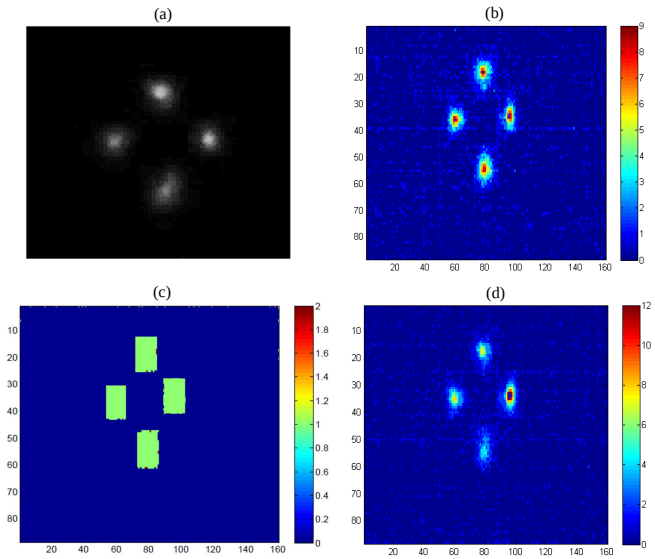

Fig. 4. (a) The raw experimental data in form of 4-spots recorded by a fast CCD camera installed at the telescope focal length. (b) Intensity thresholding of 4-spots in Matlab software. (c) Position thresholding of spots by square 12×12 windows. (d) A rarely Data fading which leads to an unfavorable frame and must be omited in the data analysis.

where N_γ is the flux from a zero magnitude star, M^V is the magnitude of star, t_{exp} is the exposure time, B_{nm} is the effective passband, QE is the quantum efficiency of the CCD camera, D is the sub-apertures diameter, and T is the optical transmission. If the star image covers an area of 11×11 CCD pixels in each sub-aperture and the peak falls on the centre of 4 CCD pixels, then each of those 4 pixels will contain 8% of the total light received from star which must be 4 or 5 times the RMS of the background level of the CCD in order to have a reliable centroiding algorithm. By assuming the $N_\gamma = 10^4$ photon $s^{-1}nm^{-1}cm^{-2}$, $M^V = 0.08$ for the Capella star, $t_{exp} = 0.0015\,s$, $B_{nm} = 300\,nm$ and $QE \times T = 0.3$, we found that $D = 3$ cm would have led to enough light about $n_e = 500$ which is 5 times the background level. Although, considering the short-exposure imaging and the scintillation effects, we choose the sub-apertures diameter $D = 10$ cm to achieve good signals, which the condition $B \geq 2D$ is also satisfied and the spots have no correlation with respect to one another. The experimental data included totally 157,000 frames is obtained by a 4-aperture mask with $B = 20.5$ cm and $D = 10$ cm and the analysis of image frames demonstrates that the median signal-to-noise ratio is about 6 which verifies the data validation.

E. Errors Analysis

one of the error sources is related to statistical errors. Because of short-exposure imaging, N samples are considered statistically independent and the time length of sampling is short enough that the image motion statistical properties remain constant. Then, according to Frieden [39], the statistical error is

$$\frac{\delta\sigma_*^2}{\sigma_*^2} = \sqrt{\frac{2}{N-1}}, \tag{13}$$

where σ_*^2 is the variance of the differential motion and so, more samples lead to smaller errors. In the following, using the Equations from section 2, the turbulence parameters estimation errors are obtained by

$$\frac{\delta r_{0,DIMM}}{r_{0,DIMM}} = \frac{\delta r_{0,4-DIMM}}{r_{0,4-DIMM}} = \frac{3}{5}\frac{\delta\sigma_*^2}{\sigma_*^2}, \tag{14}$$

$$\frac{\delta \overline{v}}{\overline{v}} = \frac{1}{2}\frac{\delta\sigma_*^2}{\sigma_*^2}, \tag{15}$$

$$\frac{\delta \tau_0}{\tau_0} = \frac{11}{10}\frac{\delta\sigma_*^2}{\sigma_*^2}. \tag{16}$$

Here, we are using image sequences of $N = 1000$ frames. Therefore, the statistical error of variance becomes $\frac{\delta\sigma_*^2}{\sigma_*^2} = 4.4\%$. Subsequently, the turbulence parameters estimation errors are calculated as $\frac{\delta r_0}{r_0} = 2.6\%$, $\frac{\delta \overline{v}}{\overline{v}} = 2.2\%$ and $\frac{\delta \tau_0}{\tau_0} = 4.9\%$.

Another source of error is stemmed from the centroid algorithm which can be affected by the CCD readout noise. In windowing technique, only the pixels within a certain radius of the image centre are used in centroid calculation as $X_w = \frac{\sum_{window} X_{ij} I_{ij}}{\sum_{window} I_{ij}}$, which we can derive the readout noise variance by $\sigma_R^2 = \frac{R^2}{I_{tot}^2}\sum_{window}(X_{ij} - \overline{X})^2$, where R is the RMS readout noise and I_{tot} is the total flux in the window. The calculation shows that σ_R^2 is very small with respect to $\sigma_{C_4}^2$ and therefore we ignore it. By considering the readout noise, the statistical and centroid errors as investigated above, the image processing and data analysis demonstrated that the image frames appear to be sound and various errors existing in sampling and calculation were tiny and insignificant.

4. DATA ANALYSIS AND RESULTS

We have collected a 157-sets of data including 1000 frames of 4-spot images from Capella star by 4-aperture DIMM instrument. Using the conventional DIMM and 4-aperture DIMM from Eqs.(3), (4), and (9), the Fried parameter r_0 is estimated as shown in Figs. 5(a) and 5(b). A comparison of conventional and 4-aperture DIMM methods shows a good consistence in results. In the following, the analysis of the velocity of the wavefront defocus includes the essential statistical data on the averaged wind speed over the turbulent layers [35]. Measuring the defocus velocity variance $\sigma^2_{\partial C_4/\partial t}$ from the 4-spot data, r_0 from above and substituting the geometrical 4-aperture mask parameters B and D into the Eq.(10), the averaged wind speed ($\overline{v}_{4-DIMM}$ or v^*) over the turbulent layers will be obtained, as shown in Figs.5(c) and 5(d). Finally, according to the atmospheric turbulence parameters r_0 and v^* estimated above, the atmospheric coherence time τ_0 is estimated from Eq.(2), as shown in Fig.6. In a word, the experimental data from 4-DIMM instrument measurement and using the 4-aperture defocus velocity theory led to estimations of r_0=8 to 16 cm, $\overline{v}$=10 to 25 m/s and τ_0=1.7 to 4 ms.

Prior to discussing the method, we would like to compare the results with lopez method which the averaged wind speed $\overline{v}_{Lopez}$ and the boiling velocity $\overline{\Delta v}$ were obtained as follows [21]

$$\overline{v}_{Lopez} = \Big[\frac{2\big(\sigma^2_{\partial\alpha/\partial t,\theta=0} - \sigma^2_{\partial\alpha/\partial t,\theta=90}\big)}{0.512\lambda^2 r_0^{-5/3} D^{-7/3}}\Big]^{1/2}, \tag{17}$$

$$\overline{\Delta v} = \Big[\frac{2\big(\sigma^2_{\partial\alpha/\partial t,\theta=0} - 3\sigma^2_{\partial\alpha/\partial t,\theta=90}\big)}{1.024\lambda^2 r_0^{-5/3} D^{-7/3}}\Big]^{1/2}, \tag{18}$$

where $\sigma^2_{\partial\alpha/\partial t}$ is the tilt velocity variance, θ is the angle of wind speed direction made by x axis and D is the aperture diameter. For an unfrozen turbulence, we have [29, 30]

$$\overline{v} \le v^* \le \sqrt{\overline{v}^2 + \overline{\Delta v}^2}, \tag{19}$$

where v^* ($\overline{v}_{5/3}$) is between the lower bound $v^*_{lower} = \overline{v}$ and upper bound $v^*_{upper} = \sqrt{\overline{v}^2 + \overline{\Delta v}^2}$ and must be substituted into Eq.(2) to achieve the atmospheric coherence time τ_0. According to Fig.7, the most striking result to emerge from the data is that the estimated $\overline{v}_{4-DIMM}$ is between the v^*_{lower} and v^*_{upper} provided by the Lopez method, and the findings suggest that the atmospheric turbulence is not frozen and the boiling velocity $\overline{\Delta v}_{boiling}$ has a great effect on v^* value. As explained above, in contrary to the Lopez method which only estimates the lower and upper limits of v^*, the method here presents a direct and accurate estimation of averaged wind speed ($\overline{v}_{4-DIMM}$ or v^*) over different atmospheric layers which leads to an accurate estimation of τ_0.

5. CONCLUSION

Our goal was to estimate the turbulence parameters r_0, $\overline{v}$ and τ_0 by a potable 4-aperture DIMM instrument. The data sampling was done at INO site by 4-DIMM instrument leading to the 4-spots displacements measurements and subsequently the 4-aperture defocus aberration calculation. The data analysis and image processing demonstrated that the image frames appear to be sound and various errors existing in sampling and calculation were tiny and insignificant.

Broadly speaking, in a conventional DIMM, the baseline must be perpendicular to the wind speed direction and so, we need

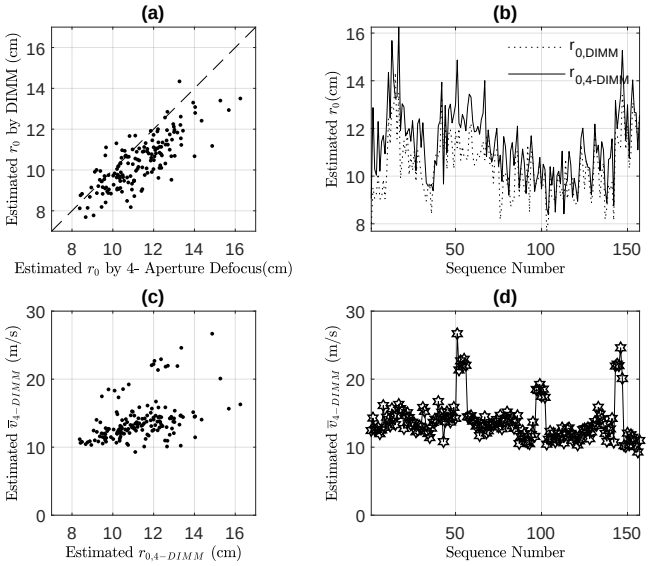

Fig. 5. (a) A comparison of conventional and 4-aperture DIMM methods in Fried parameter r_0 estimation. (b) Fluctuations of r_0 as estimated by DIMM and 4-DIMM methods. (c) Averaged wind speed $\overline{v}_{4-DIMM}$ estimations versus to estimated $r_{0,4-DIMM}$. (d) Fluctuations of averaged wind speed $\overline{v}_{4-DIMM}$ as estimated by 4-DIMM method. Atmospheric turbulence data observed at the INO on 6 September 2018 (2:15 am to 4:45 am). The experimental data includes totally 157,000 frames consisted of 157 sets of 1000 frames.

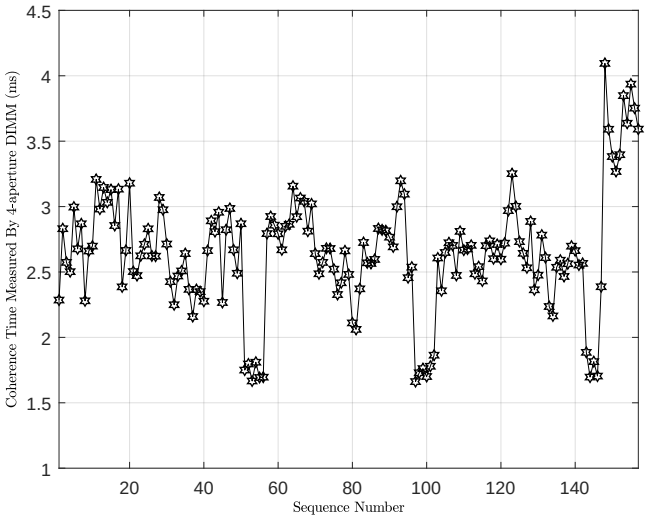

Fig. 6. Fluctuations of the atmospheric coherence time τ_0 estimated by the 4-aperture DIMM instrument. Atmospheric turbulence data observed at the INO on 6 September 2018 (2:15 am to 4:45 am). The experimental data includes totally 157,000 frames consisted of 157 sets of 1000 frames.

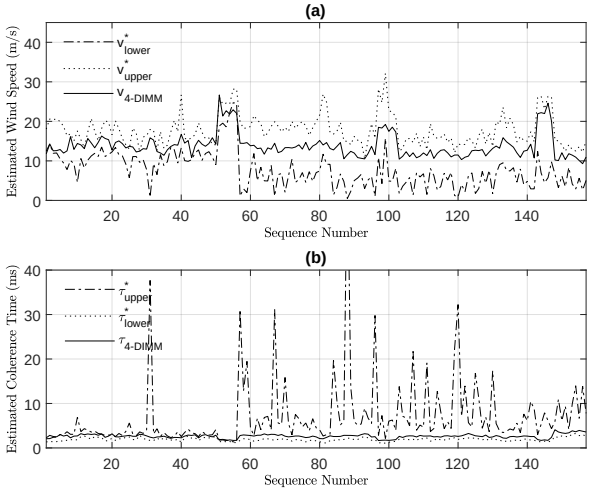

Fig. 7. A comparison of the 4-aperture DIMM method with the Lopez method to estimate the (a) averaged wind speed v^* and (b) atmospheric coherence time τ_0. v^*_{lower} and v^*_{upper} refer to lower bound and upper bound of v^* respectively estimated by the Lopez method and $\overline{v}_{4-DIMM}$ refers to $v^*(or\,\overline{v}_{5/3})$ estimated by 4-aperture DIMM method . τ^*_{lower} and τ^*_{upper} refer to lower bound and upper bound of τ_0 respectively estimated by the Lopez method and τ_{4-DIMM} refers to τ_0 estimated by 4-aperture DIMM method. Atmospheric turbulence data observed at the INO on 6 September 2018 (2:15 am to 4:45 am). The experimental data includes totally 157,000 frames consisted of 157 sets of 1000 frames.

to know the direction. But, it could be reasonably argued that the symmetry in 4-aperture DIMM caused to achieve accurate and debiased results in turbulence parameter estimation. In this work, the main important issue was the $\overline{v}$ estimation. In most of researches the averaged wind speed $\overline{v}$ is measured by other instruments or methods, or maybe the measured $\overline{v}$ is related to atmospheric surface layers. Put bluntly, we estimated the averaged wind speed v^* ($\overline{v}_{5/3}$) over different atmospheric layers directly by 4-aperture defocus velocity theory, simultaneous to r_0 estimation. In the following, using the r_0 and $\overline{v}$ estimations, the atmospheric coherence time τ_0 was obtained by Roddier relation. The measurements made by our 4-DIMM instrument and using the 4-aperture defocus velocity theory led to median estimation of $r_0 = 12cm$, $\overline{v} = 13m/s$ and $\tau_0 = 2.5ms$. In accordance with the results, we found that they were in a good agreement with the theory and simulation described in our previous work [35]. In the following, a detailed comparison with Lopez [21, 29, 30] method verified our unique approach and revealed the superiority of the method. To take the analogy further, a comparison to other studies [25, 26, 40–43], however the locations of sampling are different, but demonstrated that the results are satisfactory and consistent with other typical works.

ACKNOWLEDGMENTS

We would like to thank Dr. Habib Khosoroshahi of the INO for a fruitful collaboration that produced the experimental data and special thanks to Dr. Arash Danesh for his technical support.

REFERENCES

1. F. Roddier, "The effects of atmospheric turbulence on the formation of visible and infrared images," J. Opt. **10**, 299–303 (1979).
2. F. Roddier, "The effects of atmospheric turbulence in optical astronomy," Progr. Opt. **19**, 281–376 (1981).
3. R. k. Tyson, ed., *Priciples of Adaptive Optics* (CRC Press,Taylor Francis Group, United State of America, 2011), 1st ed.
4. R. k. Tyson, ed., *Adaptive Optics Engineering Handbook* (Marcel Dekker, New York, NY 10016, 2000), 1st ed.
5. J. E. Pearson, "Atmospheric turbulence compensation using coherent optical adaptive techniques," Appl. Opt. **15**, 622–631 (1976).
6. L. B. Stotts, ed., *Free Space Optical Systems Engineering* (Wiley, United State of America, 2017), 1st ed.
7. A. k. Majumdar, ed., *Advanced Free Space Optics(FSO)* (Springer, Ridgecrest, CA 93555 USA, 2015), 1st ed.
8. J.-P. Laussade, A. Yariv, and J. Comly, "Optical communication through random atmospheric turbulence," Appl. Opt. **8**, 1607–1611 (1969).
9. D. M. Brown, J. C. Juarez, and A. M. Brown, "Laser differential image-motion monitor for characterization of turbulence during free-space optical communication tests," Appl. Opt. **52**, 8402–8410 (2013).
10. M. M. Weiner, "Atmospheric turbulence in optical surveillance systems," Appl. Opt. **6**, 1984–1991 (1967).
11. J. Chabé, F. Blary, A. Ziad, J. Borgnino, Y. Fanteï-Caujolle, A. Liotard, and F. Falzon, "Optical turbulence in confined media: part i, the indoor turbulence sensor instrument," Appl. Opt. **55**, 7068–7077 (2016).
12. F. Blary, J. Chabé, A. Ziad, J. Borgnino, Y. Fanteï-Caujolle, A. Liotard, and F. Falzon, "Optical turbulence in confined media. part ii:first results using the intense instrument," Appl. Opt. **56**, 6272–6282 (2017).
13. J. Stock and G. Keller, *Astronomical Seeing* (the University of Chicago Press, 1961), p. 138.
14. M. G. Miller and P. Kellen, eds., *Astronomical Differential Angle of Arrival Measurement; Top. Meet. on Imaging in Astronomy* (Cambridge, Ma, 1975).
15. D. L. Fried, "Differential angle of arrival: Theory, evaluation, and measurement feasibility," Radio Science **10**, 71–76.
16. M. Sarazin and F. Roddier, "The eso differential image motion monitor," Astron. Astrophys. **19**, 294–300 (1990).
17. Aristidi, E., Agabi, A., Vernin, J., Azouit, M., Martin, F., Ziad, A., and Fossat, E., "Antarctic site testing: First daytime seeing monitoring at dome c," Astron. Astrophys. **406**, L19–L22 (2003).
18. A. V. Sergeyev and M. C. Roggemann, "Monitoring the statistics of turbulence: Fried parameter estimation from the wavefront sensor measurements," Appl. Opt. **50**, 3519–3528 (2011).
19. F. Roddier, J. M. Gilli, and G. Lund, "On the origin of speckle boiling and its effects in stellar speckle interferometry," Journal of Optics **13**, 263–271 (1982).
20. C. Aime, J. Borgnino, F. Martin, R. Petrov, G. Ricort, and S. Kadiri, "Contribution to the space–time study of stellar speckle patterns," J. Opt. Soc. Am. A **3**, 1001–1009 (1986).
21. B. Lopez, "How to monitor optimum exposure times for high resolution imaging modes?" Astron. Astrophys. **253**, 635–640 (1992).
22. R. Conan, J. Borgnino, A. Ziad, and F. Martin, "Analytical solution for the covariance and for the decorrelation time of the angle of arrival of a wave front corrugated by atmospheric turbulence," J. Opt. Soc. Am. A **17**, 1807–1818 (2000).
23. A. Ziad, R. Conan, A. Tokovinin, F. Martin, and J. Borgnino, "From the grating scale monitor to the generalized seeing monitor," Appl. Opt. **39**, 5415–5425 (2000).
24. A. Kellerer and A. Tokovinin, "Atmospheric coherence times in interferometry: Definition and measurement," Astron. Astrophys. (2007). [Astron. Astrophys.461,775(2007)].
25. A. Tokovinin, A. Kellerer, and V. Coudé du Foresto, "FADE, an instrument to measure the atmospheric coherence time," Astron. Astrophys. **477**, 671–680 (2008).
26. V. Kornilov and B. Safonov, "Differential image motion in the short-exposure regime," Mon. Not. R. Astron. Soc. **418**, 1878–1888 (2011).
27. A. Ziad, J. Borgnino, W. D. Ali, A. Berdja, J. Maire, and F. Martin, "Temporal characterization of atmospheric turbulence with the generalized

seeing monitor instrument," Journal of Optics **14**, 045705 (2012).
28. B. M. Welsh and S. C. Koeffler, "Remote sensing of atmospheric turbulence and transverse winds from wave-front slope measurements from crossed optical paths," Appl. Opt. **33**, 4880–4888 (1994).
29. B. Lopez and M. Sarazin, "Optimum Exposure Times for Interferometry," in "European Southern Observatory Conference and Workshop Proceedings," , vol. 39 of *European Southern Observatory Conference and Workshop Proceedings* J. M. Beckers and F. Merkle, eds. (1992), vol. 39 of *European Southern Observatory Conference and Workshop Proceedings*, p. 1039.
30. B. Lopez and M. Sarazin, "The ESO atmospheric temporal coherence monitor dedicated to high angular resolution imaging," Astron. Astrophys. **276**, 320 (1993).
31. R. Shomali, A. Darudi, and S. Nasiri, "Experimental measurement of the atmospheric primary aberrations by a four-aperture differential image motion monitor," Journal of Optics **15**, 125721 (2013).
32. R. Shomali, S. Nasiri, and A. Darudi, "Measurement of the atmospheric primary aberrations by a 4-aperture differential image motion monitor," Journal of Optics **13**, 055708 (2011).
33. E. M. Razi and S. Rasouli, "Measuring significant inhomogeneity and anisotropy in indoor convective air turbulence in the presence of 2d temperature gradient," Journal of Optics **16**, 045705 (2014).
34. E. M. Razi and S. Rasouli, "Investigation of inhomogeneity and anisotropy in near ground layers of atmospheric air turbulence using image motion monitoring method," Optics Communications **383**, 4444 (2016).
35. M. Panahi, R. Shomali, and M. Mollabashi, "Use of 4-aperture dimm instrument for atmospheric coherence time estimation: An analytical development," J. Opt. Soc. Am. **36**, 655–664 (2019).
36. S. Saha, *Aperture Synthesis: Methods and Applications to Optical Astronomy*, Astronomy and Astrophysics Library (Springer New York, 2010).
37. B. Dibaee, R. Shomali, J. Khalilzadeh, A. Jafari, and M. Amniat-Talab, "4-aperture differential image motion monitor as a new approach for estimating atmospheric turbulence parameters," Journal of Modern Optics **66**, 753–763 (2019).
38. J. Bally, D. Theil, Y. Billawalla, D. Potter, R. F. Loewenstein, F. Mrozek, and J. Lloyd, "A hartmann differential image motion monitor (h-dimm) for atmospheric turbulence characterisation," Publications of the Astronomical Society of Australia **13**, 22–27 (1995).
39. B. R. Frieden, ed., *Probability, Statistical Optics, and Data Testing* (Springer Berlin Heidelberg, New York, 1983), 2nd ed.
40. J. Davis and W. Tango, "Measurement of the atmospheric coherence time," Publications of the Astronomical Society of the Pacific **108**, 456 (1996).
41. Dali Ali, W., Ziad, A., Berdja, A., Maire, J., Borgnino, J., Sarazin, M., Lombardi, G., Navarrete, J., Vazquez Ramio, H., Reyes, M., Delgado, J. M., Fuensalida, J. J., Tokovinin, A., and Bustos, E., "Multi-instrument measurement campaign at paranal in 2007 - characterization of the outer scale and the seeing of the surface layer," Astron. Astrophys. **524**, A73 (2010).
42. F. Lascaux, G. Lombardi, and E. Masciadri, "On the comparison between MASS and generalized-SCIDAR techniques," Mon. Not. R. Astron. Soc. **438**, 983–1004 (2014).
43. A. Ziad, B. Chauvineau, C. Renaud, F. Morand, F. Ubaldi, J. Borgnino, P. Assus, T. Corbard, R. Ikhlef, M. Fodil, T. Abdelatif, A. Hauchecorne, G. Poiet, M. Meftah, P. Lesueur, and M. Hamadouche, "MISOLFA: a generalized monitor for daytime spatio-temporal turbulence characterization," Mon. Not. R. Astron. Soc. **458**, 517–530 (2016).